Journal of Materials Chemistry

Cite this: J. Mater. Chem., 2012, 22, 3117

www.rsc.org/materials

PAPER

Nonequilibrium structure of Zn_2SnO_4 spinel nanoparticles

Vladimir Šepelák,†*[ab] Sebastian M. Becker,[ac] Ingo Bergmann,[d] Sylvio Indris,[a] Marco Scheuermann,[a] Armin Feldhoff,[be] Christian Kübel,[a] Michael Bruns,[f] Ninette Stürzl,[a] Anne S. Ulrich,[cgh] Mohammad Ghafari,[a] Horst Hahn,[ac] Clare P. Grey,[ij] Klaus D. Becker[bk] and Paul Heitjans[be]

Received 25th October 2011, Accepted 6th December 2011
DOI: 10.1039/c2jm15427g

Zinc stannate (Zn_2SnO_4) nanoparticles with an average size of about 26 nm are synthesized *via* single-step mechanochemical processing of binary oxide precursors (ZnO and SnO_2) at ambient temperature, without the need for the subsequent calcination, thus making the synthesis route very simple and cost-effective. The mechanically induced phase evolution of the $2ZnO + SnO_2$ mixture is followed by XRD and by a variety of spectroscopic techniques including ^{119}Sn MAS NMR, Raman spectroscopy, ^{119}Sn Mössbauer spectroscopy, and XPS. High-resolution TEM studies reveal a non-uniform structure of mechanosynthesized Zn_2SnO_4 nanoparticles consisting of a crystalline core surrounded by a structurally disordered surface shell. Due to the ability of the applied solid-state spectroscopies to probe the local environment of Sn cations, valuable complementary insight into the nature of the local structural disorder of mechanosynthesized Zn_2SnO_4 is obtained. The findings hint at a highly nonequilibrium state of the as-prepared stannate characterized by its partly inverse spinel structure and the presence of deformed polyhedra in the surface shell of nanoparticles.

Introduction

Interest in ternary tin-based oxides (stannates) of the type M_2SnO_4 (M is a divalent metal cation) has greatly increased in the past few years because of their potential applications, such as photoelectrical devices,[1] chemical sensors,[2] functional coatings,[3] transparent conducting electrodes,[4] anode materials in Li-ion batteries,[5] and photocatalysts.[6] Zinc stannate, Zn_2SnO_4, is an important member of the stannate family. It is noteworthy for its transparency in the visible light region and a relatively high electrical conductivity. As a transparent n-type semiconducting oxide, this material is characterized by a band gap of 3.6 eV and electron mobility of 10–15 $cm^2\ V^{-1}\ s^{-1}$.[7] In the bulk state, Zn_2SnO_4 is known to be a fully inverse 2–4 cubic spinel (where 2–4 refers to the valences of Zn and Sn cations) with the unit cell parameter $a =$ 8.6574 Å and space group $Fd3m$ (JCPDS PDF 24-1470).[8] To emphasize the site occupancy at the atomic level, the structural formula of this spinel may be written as $(Zn^{2+})[Sn^{4+}Zn^{2+}]O_4$, where parentheses and square brackets enclose cations in sites of tetrahedral (A) and octahedral [B] coordination, respectively. Note that despite their deceptively simple structure (Fig. 1), many spinel oxides exhibit complex disordering phenomena involving the redistribution of cations over the (A) and [B] sublattices provided by the spinel structure.[9,10]

It is widely appreciated that the performance of transparent conducting oxides, including that of Zn_2SnO_4, is closely related to the ways in which they are processed. The conventional solid-state (ceramic) synthesis of Zn_2SnO_4 requires prolonged treatment of the reaction precursors at considerably high calcination temperatures.[11] In many cases, this causes the loss of zinc due to its high volatility and, consequently, it results in the formation of multiphase products[12] and the degradation of microstructural and functional properties of the stannate material. Various wet chemistry-based routes have also been developed to synthesize

[a]*Institute of Nanotechnology, Karlsruhe Institute of Technology, Hermann-von-Helmholtz-Platz 1, D-76344 Eggenstein-Leopoldshafen, Germany. E-mail: vladimir.sepelak@kit.edu; Fax: +49-721-60826368; Tel: +49-721-60828929*
[b]*Center for Solid State Chemistry and New Materials, Leibniz University Hannover, Callinstr. 3-3A, D-30167 Hannover, Germany*
[c]*DFG Center for Functional Nanostructures, Karlsruhe Institute of Technology, Wolfgang-Gaede-Str. 1A, D-76131 Karlsruhe, Germany*
[d]*Volkswagen AG, D-38436 Wolfsburg, Germany*
[e]*Institute of Physical Chemistry and Electrochemistry, Leibniz University Hannover, Callinstr. 3-3A, D-30167 Hannover, Germany*
[f]*Institute for Applied Materials (IAM-WPT), Karlsruhe Institute of Technology, Hermann-von-Helmholtz-Platz 1, D-76344 Eggenstein-Leopoldshafen, Germany*
[g]*Institute of Organic Chemistry, Karlsruhe Institute of Technology, Fritz-Haber-Weg 6, D-76131 Karlsruhe, Germany*
[h]*Institute of Biological Interfaces (IBG-2), Karlsruhe Institute of Technology, Hermann-von-Helmholtz-Platz 1, D-76344 Eggenstein-Leopoldshafen, Germany*
[i]*Chemistry Department, State University of New York, Stony Brook, New York, 11794-3400, USA*
[j]*Chemistry Department, University of Cambridge, Lensfield Rd, Cambridge, CB2 1EW, UK*
[k]*Institute of Physical and Theoretical Chemistry, Braunschweig University of Technology, Hans-Sommer-Str. 10, D-38106 Braunschweig, Germany*
† On leave from the Slovak Academy of Sciences, 04353 Košice, Slovakia.

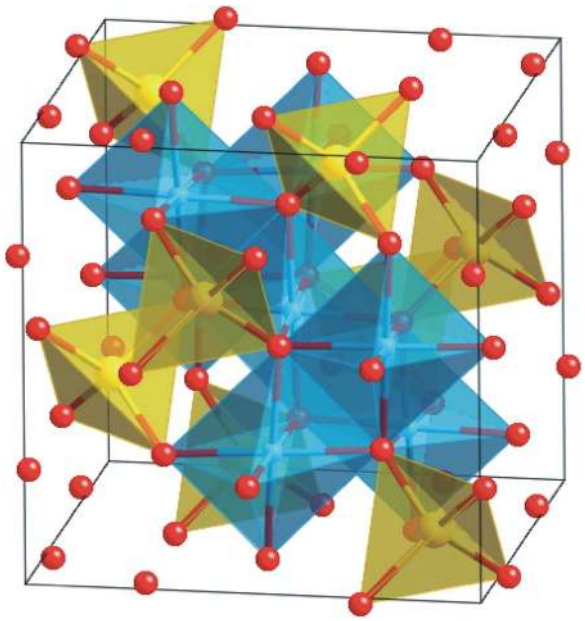

Fig. 1 The cubic spinel structure of Zn_2SnO_4. Zn^{2+} and Sn^{4+} cations are distributed over the sites of tetrahedral (A) and octahedral [B] coordination. In the bulk material, one-half of Zn^{2+} ions occupies (A) sites, whereas Sn^{4+} cations and the other half of Zn^{2+} ions occupy [B] sites. Thus, the crystal chemical formula of the Zn_2SnO_4 spinel, emphasizing the site occupancy at the atomic level, may be written as $(Zn^{2+})[Sn^{4+}Zn^{2+}]O_4$.

nanosized Zn_2SnO_4 powders.[1–6] However, most of the solution chemistry-based routes still involve calcinations, although at relatively lower temperatures.[1] The non-conventional *mechanochemical synthesis* (mechanosynthesis) has been recognized as an alternative route overcoming all of these problems and providing an efficient one-step and facile access to nanomaterials.[13] In the past years, a surge of investigations in the field of *mechanochemistry* have clearly demonstrated that a variety of complex oxides, including stannates,[14,15] can be synthesized at ambient temperature directly from their precursors in the form of nanosized powders, without the need for the calcination at intermediate temperatures, thus making the process very simple and cost-effective.

In this context, the present work is focused on the one-step synthesis of nanocrystalline Zn_2SnO_4 *via* mechanochemical processing of a $2ZnO + SnO_2$ mixture at ambient temperature. Although the mechanosynthesis of Zn_2SnO_4 has already been reported in a few papers,[16] to the best of our knowledge there is no report in the literature on the defect state or the disordered local structure of Zn_2SnO_4 prepared by the non-conventional mechanochemical route. Moreover, in the above-mentioned papers the formation of mechanosynthesized Zn_2SnO_4 has only been established by X-ray diffraction (XRD). As it is clearly demonstrated in our work on the mechanosynthesis of ternary complex oxides,[14,17–19] solely from the XRD measurements, it is not clear whether the mechanochemical processing of a mixture of reaction precursors leads to the complete conversion to a complex oxide, even if the diffraction patterns of the milled powders exhibit typical features of a desired phase. According to our experience,[14,17–22] the simultaneous use of diffraction techniques, which are sensitive to medium- and long-range structural order, and spectroscopic techniques such as nuclear magnetic resonance (NMR), Raman spectroscopy and/or Mössbauer spectroscopy, which make possible observations on a local atomic scale, is indispensable in many cases to allow for a comprehensive characterization of the product of a mechanochemical reaction.

Thus, in this article, detailed information is obtained on the short-range local structure of nanocrystalline Zn_2SnO_4 synthesized completely in a one-step mechanochemical process. In addition to XRD, the phase evolution during the mechanosynthesis as well as the far-from-equilibrium structural state of the reaction product are systematically monitored with a variety of comprehensive spectroscopic techniques including ^{119}Sn magic angle spinning (MAS) NMR, Raman spectroscopy, ^{119}Sn Mössbauer spectroscopy, and X-ray photoelectron spectroscopy (XPS). The morphology of mechanosynthesized Zn_2SnO_4 nanoparticles is studied by transmission electron microscopy (TEM).

Experimental section

For the mechanochemical synthesis of Zn_2SnO_4, the ZnO and SnO_2 reactants (Merck, Darmstadt, Germany) were mixed in a molar ratio of 2 : 1 and used as starting materials. The $2ZnO + SnO_2$ mixtures (7 g) were milled for various times t_m (up to 4 h) in a Fritsch Pulverisette 7 Premium Line planetary ball mill (Fritsch, Idar-Oberstein, Germany) at room temperature. A grinding chamber (45 cm^3 in volume) and balls (10 mm in diameter) made of tungsten carbide were used. The ball-to-powder weight ratio was 20 : 1. Milling experiments were performed in air at 800 rpm.

Additionally, bulk Zn_2SnO_4 (polycrystalline stannate with an average crystallite size exceeding 100 nm), which served as a reference sample in this study, was prepared from stoichiometric amounts of reagent-grade precursors (ZnO and SnO_2) by the conventional ceramic route. Powdered reactants were at first homogenized and then pressed into tablets in order to obtain a high degree of compaction. The reaction tablets were prefired at 1373 K for 24 h, reground, pressed, and finally sintered at 1373 K for 24 h.

The XRD patterns were measured using a STOE STADI P X-ray diffractometer (STOE, Germany), operating in Bragg configuration and using Cu Kα radiation (1.5405 Å). The XRD scans were collected from 10° to 80° (2Θ), using a step of 0.02° and a data collection time of 5 s. The JCPDS PDF database[8] was utilized for phase identification using the STOE software. The cubic spinel structure of Zn_2SnO_4 was visualized using the Diamond program.[23]

The morphology of powders was studied using a combined field-emission (scanning) transmission electron microscope (S)TEM (JEOL JEM-2100F) and an image corrected microscope FEI Titan 80-300. An energy-dispersive X-ray (EDX) spectrometer (Oxford Instruments INCA 200 TEM) with an ultra-thin window allowed for chemical analysis within grains of the mechanosynthesized material. Prior to TEM investigations, powders were crushed in a mortar, dispersed in ethanol, and fixed on a copper-supported carbon grid.

^{119}Sn MAS NMR measurements were performed on an Avance 500 spectrometer (Bruker, Germany). A rotor-synchronized spin–echo pulse sequence was used to avoid dead-time

effects during data acquisition. Typically, 200 scans were acquired with a repetition delay of 60 s. The magnetic field of 11.8 T was used, which corresponds to a Larmor frequency of $\nu_L = 186.3$ MHz. The milled $2ZnO + SnO_2$ mixtures and the bulk Zn_2SnO_4 sample were rotated in 2.5 mm- and 3.2 mm-rotors at a spinning speed of 35 and 24 kHz, respectively. ^{119}Sn NMR spectra were referenced to microcrystalline SnO_2 with an isotropic chemical shift of −604 ppm.[24]

Room-temperature Raman spectra were acquired using a HoloSpec Raman spectrometer (Kaiser Optical Systems, Inc., USA) with a laser excitation wavelength of 785 nm. The laser power was set at 10 mW.

^{119}Sn Mössbauer spectroscopic measurements were carried out in transmission mode at room temperature. ^{119}Sn-enriched $CaSnO_3$ was used as the γ-ray source. The velocity scale was calibrated relative to ^{119}Sn in $CaSnO_3$. Recoil spectral analysis software[25] was used for the quantitative evaluation of the Mössbauer spectra.

The surface analytical studies were performed using a K-Alpha XPS spectrometer (ThermoFisher Scientific, East Grinstead, UK). Data acquisition and processing using the Thermo Avantage software are described elsewhere.[26] All samples were analyzed using a microfocused, monochromated Al Kα X-ray source (spot size: 30–400 μm). The K-Alpha charge compensation system was employed during analysis, using electrons (8 eV) and low-energy argon ions to prevent any localized charge build-up. The spectra were fitted with Voigt profiles (uncertainty of the binding energy: 0.1 eV). All spectra were referenced to the C1s peak of hydrocarbon (at 285.0 eV) controlled by means of the well-known photoelectron peaks of metallic Cu, Ag, and Au.

Results and discussion

The mechanically induced evolution of the $2ZnO + SnO_2$ mixture was followed by XRD. Fig. 2 shows XRD patterns of the mixture milled for various times. For comparison, the XRD pattern of the Zn_2SnO_4 standard sample (bulk material prepared by the conventional ceramic route) is also presented at the bottom of Fig. 2. The XRD pattern of the starting powder (Fig. 2a) is characterized by sharp diffraction peaks corresponding to the reactants ZnO (JCPDS PDF 36-1451) and SnO_2 (JCPDS PDF 41-1445).[8] During the early stages of milling (for $t_m \leq 1$ h), XRD merely reveals a decrease in the intensity and an associated broadening of the Bragg peaks of the individual oxides. However, for milling times $t_m > 1$ h, qualitative changes are observed in the XRD patterns of the milled samples; clear evidence is observed of new diffraction features that correspond to the cubic Zn_2SnO_4 phase. In the XRD pattern of the sample milled for 4 h (a product of the mechanochemical reaction), all diffraction peaks detected above the background are due to the Zn_2SnO_4 phase (JCPDS PDF 24-1470).[8] The broad shape of XRD lines for mechanosynthesized stannate, in contrast to relatively narrow lines for the bulk Zn_2SnO_4 (compare lines f and g in Fig. 2), provides clear evidence of a nanoscale nature of the mechanosynthesized material.

Representative TEM micrographs of nanocrystalline mechanosynthesized Zn_2SnO_4 at low and high magnifications are shown in Fig. 3. It is revealed that the mechanosynthesized stannate consists of nanoparticles with a size distribution ranging

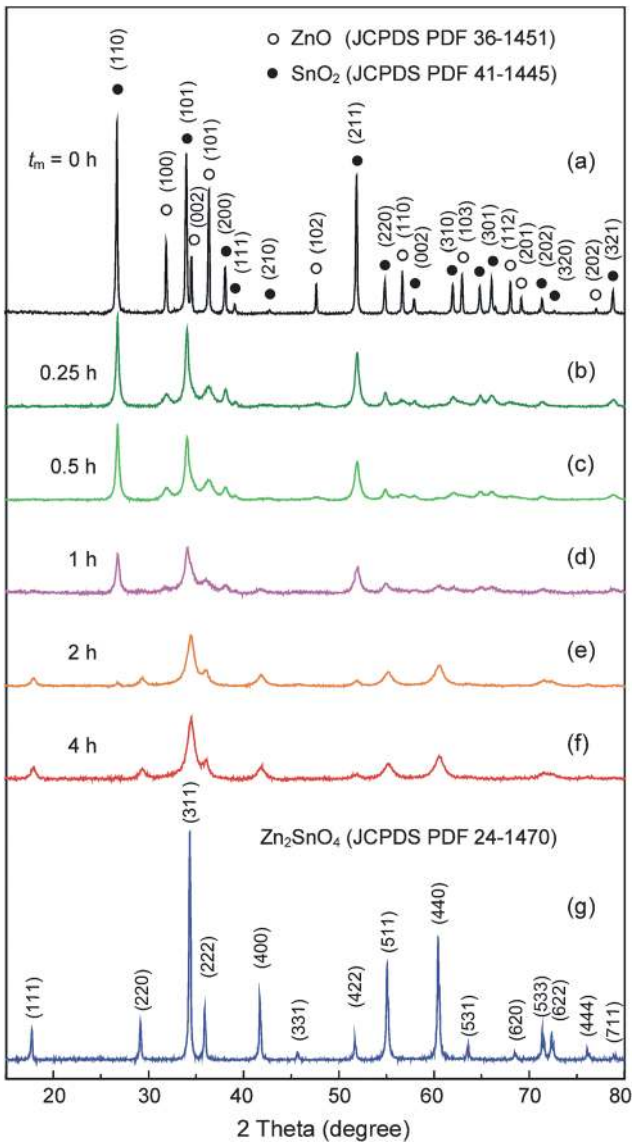

Fig. 2 XRD patterns of (a–f) the $2ZnO + SnO_2$ mixture milled for various times (up to 4 h) and of (g) the bulk Zn_2SnO_4 prepared by the conventional ceramic route. The milling times, t_m, are shown in the figure. Diffraction peaks of the reaction precursors and the bulk Zn_2SnO_4 are denoted by Miller indices. The intensity scale of the XRD patterns is normalized to that of the XRD pattern of the starting powder.

from about 5 to 40 nm; an average crystallite size is estimated to be 26(2) nm. This relatively broad distribution of particle sizes, visible in the bright-field TEM image in Fig. 3a, can be a result of the heterogeneous *nucleation-and-growth* processes[19] of the product phase in the course of the mechanically induced formation reaction. Mechanosynthesized Zn_2SnO_4 nanoparticles are found to be roughly spherical. An interesting observation is that the as-prepared nanoparticles possess the so-called *core–shell* configuration consisting of an ordered inner core surrounded by a structurally disordered surface shell region. The high-resolution TEM images (Fig. 3b and c) show lattice fringes corresponding to the crystallographic plane (220) ($d = 3.062$ Å) of the Zn_2SnO_4 phase (JCPDS PDF 24-1470).[8] The lattice fringes cross the whole particle core demonstrating the single-crystalline

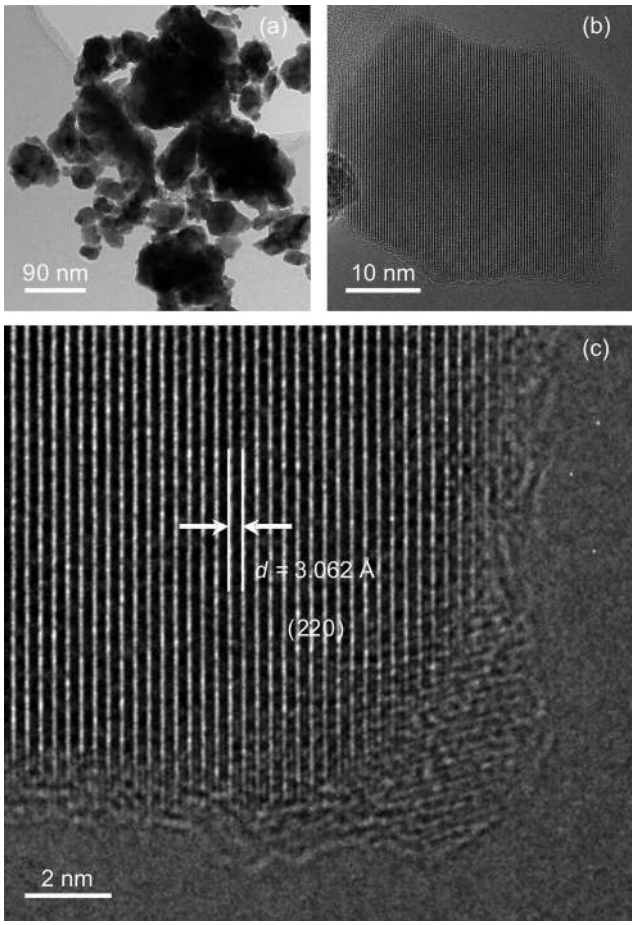

Fig. 3 (a) Bright-field and (b) high-resolution TEM images of nanocrystalline mechanosynthesized Zn_2SnO_4. (c) The core–shell configuration of mechanosynthesized nanoparticles with the thickness of the surface shell exceeding 2 nm is evident. The lattice fringes correspond to the crystallographic plane (220) (d = 3.062 Å) of the Zn_2SnO_4 phase (JCPDS PDF 24-1470).

character of the nanoparticles. The thickness of the structurally disordered surface shell estimated from high-resolution TEM is found to exceed 2 nm (Fig. 3c).

Assuming a spherical shape of Zn_2SnO_4 nanoparticles and taking both their average diameter ($D = 26$ nm) and the thickness of their surface shell (*e.g.*, t = 2.5 nm) as determined experimentally by TEM, one can easily deduce quantitative information on the volume fraction of disordered surface shell regions, w, to the volume of whole particles ($w = V_{shell}/(V_{core} + V_{shell})$) in the nanomaterial.‡ The estimated value of $w = 0.473$ indicates that about 50% of atoms in the mechanosynthesized stannate are in a structurally disordered state located in the surface shell of nanoparticles. In this context, it should be noted that the structurally non-uniform core–shell configuration of nanoparticles with the relatively large volume fraction of surface shell regions (up to about 50%) has also been reported for mechanochemically prepared spinel ferrites[17] and aluminates,[9] perovskites,[19] as well as orthorhombic and trigonal complex oxides.[14,18,27] The shell thickness in mechanosynthesized Zn_2SnO_4 nanoparticles is comparable to that observed in other nanosized mechanochemically prepared oxides.[9,14,17–19,27–29]

To determine the phase evolution of the $2ZnO + SnO_2$ mixture during high-energy milling in greater detail and to provide insight into the local structural disorder in stannate nanoparticles, the mechanochemical reaction was also followed by ^{119}Sn MAS NMR. This nuclear spectroscopic method has been proven to be exceptionally sensitive to changes in the short-range structure around the tin ions (*e.g.*, to distortions of the oxygen polyhedra) as well as to their charge state.[14,21,30] Fig. 4 compares ^{119}Sn MAS NMR spectra of the $2ZnO + SnO_2$ mixtures milled for various times with that of the bulk Zn_2SnO_4 standard. The spectrum of the initial mixture shows a sharp resonance at −604 ppm corresponding to the Sn atoms located in SnO_6 octahedra in the tetragonal structure of bulk SnO_2.[14,21,31] With increasing

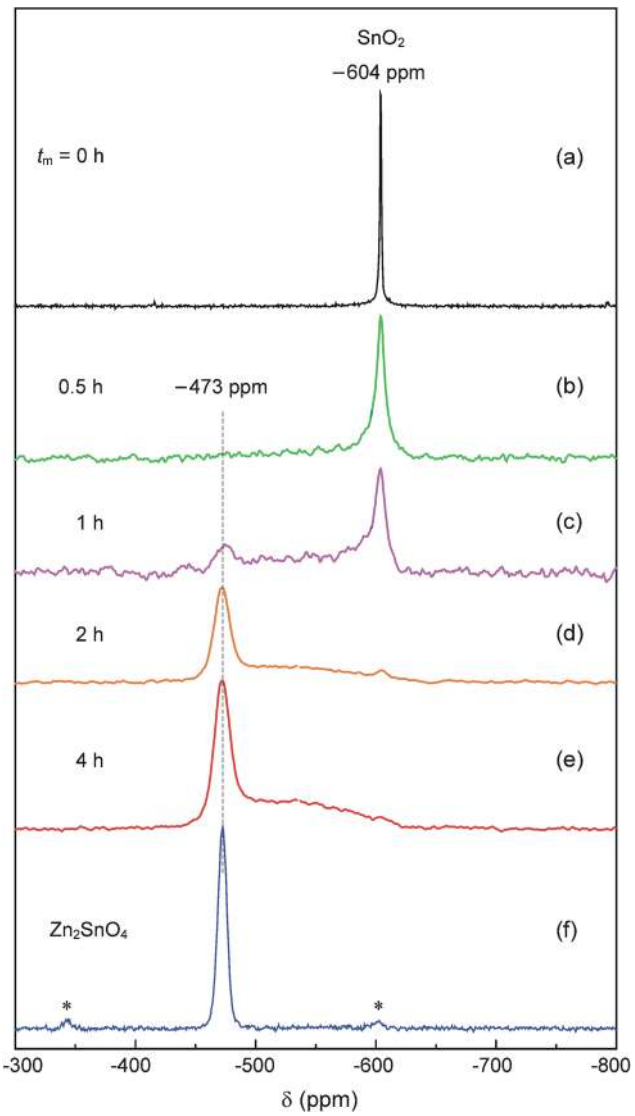

Fig. 4 ^{119}Sn MAS NMR spectra of (a–e) the $2ZnO + SnO_2$ mixture milled for various times (up to 4 h) and of (f) the bulk Zn_2SnO_4 prepared by the conventional ceramic route. The milling times, t_m, are shown in the figure. Spinning sidebands associated with the resonance at −473 ppm are marked with *.

‡ $w = [1 - (1 - 2t/D)^3]$.

milling time, the resonance line corresponding to SnO_2 broadens significantly, slowly collapses, and is gradually replaced by a new resonance line at −473 ppm. This spectral component is known to arise from octahedrally coordinated Sn^{4+} cations in Zn_2SnO_4.[24] It should be mentioned in this context that this resonance line assigned to the Zn_2SnO_4 phase is clearly visible after only 1 h of milling (see Fig. 4c). Further milling leads to a gradual increase of its relative intensity. After 4 h of milling, the resonance peak of the SnO_2 educt has disappeared completely and the NMR spectrum of the milled powder is dominated by the line at −473 ppm superimposed on a broad peak ranging from about −430 to −620 ppm (centred at −524 ppm); see Fig. 4e. Taking into account both the above-mentioned range of chemical shifts and the single phase nature of the mechanosynthesized material as revealed by XRD, the broad resonance peak can also be assigned to the Sn atoms in octahedral coordination of oxygen ions in the spinel structure of the mechanosynthesized Zn_2SnO_4. Its structural origin will be discussed in greater detail concurrently with the analysis of NMR data (see below).

The well-resolved ^{119}Sn MAS NMR subspectra corresponding to educt (SnO_2) and product (Zn_2SnO_4) phases allow an accurate determination of the degree of conversion in the course of the present mechanochemical reaction. Fig. 5 illustrates the decrease in the integral intensity of the NMR spectral line corresponding to SnO_2, I_{SnO2}, relative to the total spectral intensity, I_{tot}, reflecting a gradual conversion of the reactants to the stannate phase during milling. It is clearly seen that the mechanochemical reaction is completed after a relatively short time (4 h). Note that the presence of the product phase in the samples milled for $t_m \leq 1$ h is not registered by XRD (see Fig. 2), whereas, for the same t_m, the nucleation of the Zn_2SnO_4 phase manifests itself by the appearance of the broad resonance peak at −524 ppm in the NMR spectra (see lines b and c in Fig. 4). Correspondingly, the NMR technique reveals that the degree of conversion of the mechanochemical reaction is already about 22 and 62% for the samples milled for 0.5 and 1 h, respectively. This indicates that the energy transferred from the milling balls to the powder causes the nucleation of the Zn_2SnO_4 phase already during the early stages of milling. Moreover, this gives evidence of the fact that the NMR active ^{119}Sn nuclei provide a very sensitive probe for the estimation of the yield of the mechanochemical reaction. Thus, the combination of XRD and NMR spectroscopies provides the full information to be gained on the progress of the mechanosynthesis.

To provide more detailed information on the structural origin of the broad resonance peak centred at −524 ppm in the NMR spectrum of the mechanosynthesized material (see Fig. 6), we should recall the fact that the chemical shift of a ^{119}Sn NMR line reflects the local environment of Sn nuclei, *i.e.*, the short-range nearest-neighbour atomic structure around the tin ions. Consequently, the broad NMR peak reflects the presence of a broad distribution of local atomic environments around the octahedrally coordinated Sn cations (distorted oxygen octahedra) in the mechanosynthesized material. In this context, it should be emphasized that the presence of both regular and highly distorted SnO_6 octahedra has also been evidenced in Zn_2SnO_4 thin films by means of ^{119}Sn Mössbauer

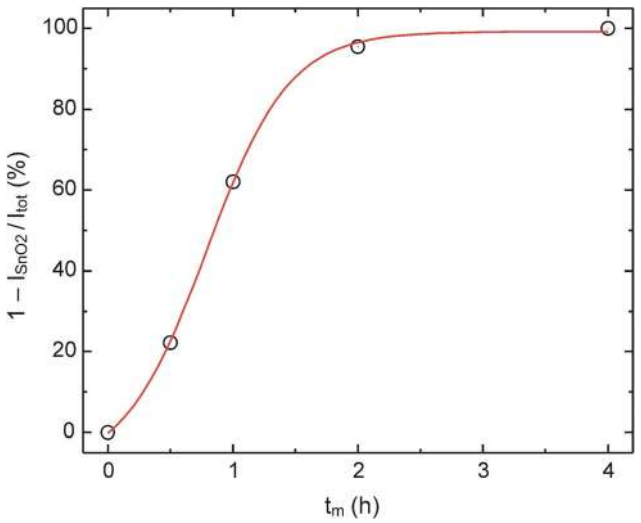

Fig. 5 Time dependent progress of reaction $2ZnO + SnO_2 \rightarrow Zn_2SnO_4$, demonstrating the complete conversion of the educt phases during the mechanochemical synthesis.

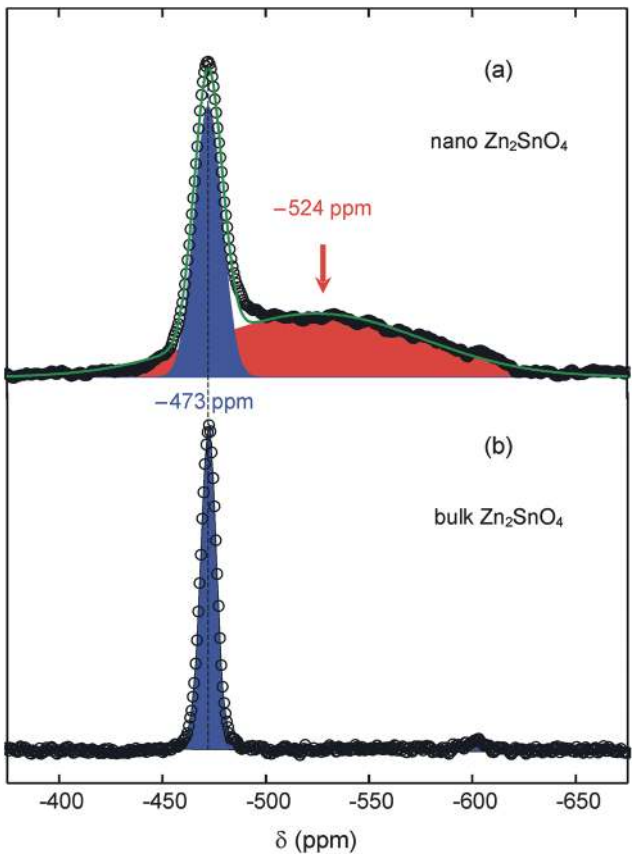

Fig. 6 ^{119}Sn MAS spectra of (a) mechanosynthesized Zn_2SnO_4 and (b) bulk Zn_2SnO_4 prepared by the conventional thermal route. The resonance line at −473 ppm arises from the octahedrally coordinated Sn ions in (a) the core of Zn_2SnO_4 nanoparticles and (b) in the bulk material, whereas the broad line centred at −524 ppm is associated with the Sn ions occupying deformed SnO_6 octahedra in the near-surface layers of nanoparticles.

spectroscopy.[32] Similar findings have also been reported for other spinel-type oxides such as aluminates,[9,33] ferrites[17] and germanates,[34] where the mechanically induced particle size reduction to the nanometre range was found to be accompanied by a deformation of polyhedron geometries. Taking into account the core–shell configuration of mechanosynthesized stannate nanoparticles evidenced by HR-TEM (see Fig. 3), it can be assumed that the deformed SnO_6 octahedra are located in the surface shell regions of the nanomaterial. This is also consistent with recent work on the mechanosynthesized orthorhombic and perovskite oxide nanoparticles, whose near-surface layers are structurally disordered due to a broadly distorted geometry of XO_6 (X = Sn, Fe) octahedra.[14,18,19] To summarize, the comparative NMR study of bulk and nanocrystalline Zn_2SnO_4 enables us to separate surface effects from bulk effects in mechanosynthesized nanoparticles; the relatively narrow resonance line at −473 ppm (see Fig. 6) is ascribed to arise from the octahedrally coordinated Sn ions in the core of Zn_2SnO_4 nanoparticles (and in the bulk material), whereas the broad line centred at −524 ppm is associated with the Sn ions occupying deformed SnO_6 octahedra in the near-surface layers of nanoparticles. Integration of the resonance peak intensities (Fig. 6a) reveals that about 50% of the Sn atoms are located in the disordered surface shell regions of the as-prepared Zn_2SnO_4 nanoparticles. This value of the volume fraction of surface shell regions determined by NMR is in reasonable agreement with that obtained by high-resolution TEM.

Information on the short-range structure of Zn_2SnO_4 nanoparticles, provided by the ^{119}Sn MAS NMR technique, is complemented by an investigation of the structural disorder of the nanomaterial on a local atomic scale by means of Raman spectroscopy. Fig. 7 displays the background-corrected Raman spectra of both mechanosynthesized and conventionally prepared zinc stannates. In the spectrum of the bulk material, the following five Raman-active modes are observed in the frequency range from 300 to 800 cm^{-1}: at 381, 467, 527, 556, and 667 cm^{-1}. These vibrational modes are in agreement with the previous measurements[35] and theoretical calculations[36] of Raman-active modes for the inverse spinel structure of Zn_2SnO_4. The modes can be reasonably assigned to $F_{2g}(1)$, E_g, $F_{2g}(2)$, $F_{2g}(3)$, and A_{1g} symmetries, respectively. It should be emphasized that the mode with the highest intensity at 667 cm^{-1} is due to the symmetric stretching of the Zn–O bonds in the ZnO_4 tetrahedra of the fully inverse Zn_2SnO_4 spinel (the so-called tetrahedral breathing mode[37]). The other four phonon modes at lower frequencies (<600 cm^{-1}) are due to a metal ion involved in [B] coordination of oxygen ions; *i.e.*, they correspond to the symmetric and asymmetric bending of oxygen atoms in the *Me*–O bonds of the MeO_6 octahedra (*Me* = Zn or Sn).[38] Note that the two first-order Raman modes with close vibrational frequencies at 527 and 556 cm^{-1} are typical of the fully inverse spinel structure of Zn_2SnO_4, and are induced by the vibrations related to Sn and Zn cations at the equal (octahedral) sites.[39]

In contrast to the conventionally prepared bulk material, the Raman spectrum of the nanocrystalline mechanosynthesized stannate exhibits an additional peak at 626 cm^{-1} (see Fig. 7). The positions of all other Raman peaks in the spectrum of the nanostannate are the same as those observed for the bulk spinel. Moreover, the spectrum of the nanomaterial shows a marked

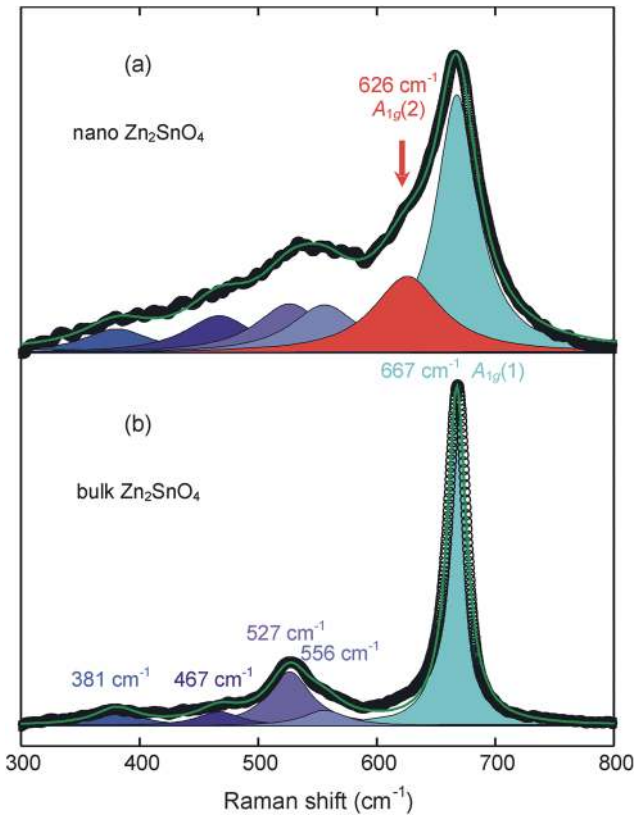

Fig. 7 Raman spectra of (a) mechanosynthesized Zn_2SnO_4 and (b) bulk Zn_2SnO_4 prepared by the conventional thermal route. The frequencies of the Raman modes are indicated in the figure. The phonon band at 626 cm^{-1} is assigned to the vibrations of the Sn–O bonds in the SnO_4 tetrahedra created by the redistribution of some Sn ions from [B] to (A) sites.

difference in relative intensity and width of the vibrational peaks when compared with those of bulk Zn_2SnO_4. To interpret these spectral features, and especially, the appearance of the additional Raman phonon mode at 626 cm^{-1}, it should be emphasized that the cation redistribution between the (A) and [B] lattice sites of a spinel crystal may alter its symmetry and manifests itself by a larger number of active vibrational modes in the Raman spectrum.[37,40] The change in cationic order in spinels is usually induced by high temperature,[41] high pressure,[42] irradiation of a material with high-energy electrons, ions or neutrons,[43] and its particle size reduction to the nanometre range.[9,33,44] Independent of the ionic configuration in spinels, all these processing parameters were found to change the cation distribution in spinels towards the random arrangement.[9,33] In analogy with the Raman results on cation redistribution in spinels induced by thermal treatment,[45] high pressure[39,42] and particle size reduction,[40] the phonon band at 626 cm^{-1}, observed exclusively in the spectrum of the mechanosynthesized Zn_2SnO_4 spinel, can be assigned as a fundamental Raman-active vibration of the Sn–O bonds in the SnO_4 tetrahedra (having A_{1g} character) created by the redistribution of some Sn ions from [B] to (A) sites. In other words, this Raman mode indicates the presence of the disorder of Sn and Zn cations over the (A) and [B] crystal sites provided by the spinel structure of nanocrystalline Zn_2SnO_4. A significantly altered relative intensity of the Raman peaks at 527 and 556 cm^{-1}

(compare spectra in Fig. 7) may also reflect a reduced concentration of Sn^{4+} cations on [B] sites and, *vice versa*, an increased population of Zn^{2+} ions on [B] sites in the nanostannate. The relatively broad Raman spectral lines for mechanosynthesized spinel, in comparison to those of the bulk oxide, imply the presence of deformed MeO_4 tetrahedra and MeO_6 octahedra (Me = Zn or Sn) in the nanospinel, as it is clearly evidenced by ^{119}Sn MAS NMR (see above).

The present comparative Raman investigation of the stannates thus indicates that, in contrast to the bulk material exhibiting the fully inverse spinel structure of the type (Zn)[SnZn]O_4, the nanocrystalline mechanosynthesized Zn_2SnO_4 adopts a partly inverse spinel structure characterized by the crystal chemical formula of $(Zn_\lambda Sn_{1-\lambda})[Sn_\lambda Zn_{2-\lambda}]O_4$, where the symbol λ represents the degree of inversion ($0 < \lambda < 1$). Note that no attempt was made to quantitatively estimate the degree of inversion from the present Raman data. The disorder of Sn and Zn cations is confined to the near-surface layers of Zn_2SnO_4 nanoparticles, *i.e.*, the inner core of nanoparticles possesses the fully inverse spinel structure ($\lambda = 1$), whereas the surface shell is disordered due to a nonequilibrium cation distribution ($\lambda \neq 1$). This is consistent with the results of previous ^{57}Fe Mössbauer and ^{27}Al MAS NMR investigations of mechanochemically prepared spinel oxides such as ferrite,[17] aluminate[9,33] and germanate nanoparticles,[34] whose near-surface layers have been found to be disordered due to the nearly *random* distribution of cations (characterized by $\lambda = 2/3$ for 2–3 and 2–4 spinels) and the deformed polyhedra. It should be emphasized that various additional structural features have been found to be characteristic for a far-from-equilibrium state of the surface shell in mechanosynthesized nanooxides. In magnetic ferrite nanoparticles, for example, the canted spin arrangement is confined to the particle's near-surface layers with the thickness extending up to about 1 nm.[17,19] In the case of the mechanosynthesized perovskites (*e.g.*, $BiFeO_3$) and trigonal nanooxides (*e.g.*, $LiNbO_3$), the surface shell regions are found to be even amorphous.[19,27]

The important impact of the present work, from the methodology point of view, is the application of a variety of spectroscopic techniques to the study of the mechanically induced formation reaction ($2ZnO + SnO_2 \rightarrow Zn_2SnO_4$). In the following, we will present the results of ^{119}Sn Mössbauer and XPS investigations of the evolution of the Zn_2SnO_4 nanophase during the mechanosynthesis. Especially, ^{119}Sn Mössbauer spectroscopy, which involves transitions between the ground and first excited nuclear state (where the latter possesses spin $I = 3/2$), can provide information on the quadrupolar interactions experienced by the nuclei of ^{119}Sn. This can complement the above-presented results of Raman and NMR spectroscopies. Note that the latter technique is concerned with the nuclear ground state of ^{119}Sn nuclei with spin $I = 1/2$ and thus exclusively reflects chemical shift interactions experienced by the nuclei. In this context, the Zn_2SnO_4 formation reaction represents an excellent model system for studies of changes in the local structure during mechanosynthesis because the tin nucleus ^{119}Sn can serve as local probe in both NMR as well as Mössbauer measurements.

Fig. 8 shows ^{119}Sn Mössbauer spectra of the $2ZnO + SnO_2$ educt mixture and the mechanosynthesized Zn_2SnO_4 product in comparison with the spectrum of bulk Zn_2SnO_4 prepared by the ceramic route. The spectrum of the starting powder is characterized by a doublet with an average isomer shift IS = −0.012(2) mm s^{-1} and a quadrupole splitting QS = 0.521(1) mm s^{-1} corresponding to octahedrally coordinated Sn^{4+} cations in the tetragonal structure of SnO_2.[14,21,46] Note that because of a relatively large Lorentzian line half-width of about 0.4 mm s^{-1}, typical of ^{119}Sn Mössbauer spectroscopy,[14] the doublet appears as a singlet (with flat bottom) in the spectrum. The isomer shift of the spectrum of mechanosynthesized Zn_2SnO_4 (IS = 0.129(6) mm s^{-1}) is very close to that of the bulk sample (IS = 0.134(8) mm s^{-1}), indicating the same electronic charge density at the Sn nuclei (*i.e.*, the presence of exclusively Sn^{4+} ions) in both stannates. On the other hand, the average quadrupole splitting for the mechanochemically synthesized Zn_2SnO_4 (QS = 0.565(7) mm s^{-1}) is significantly larger than that estimated for the conventionally prepared material (QS = 0.470(4) mm s^{-1}). This feature can reflect the presence of several overlapping subpatterns in the spectrum of the nanomaterial, associated with regular and distorted polyhedra[32] and/or with Sn^{4+} cations at the (A) and [B] spinel sites. However, because of the relatively structureless Mössbauer spectrum of the mechanosynthesized product, no attempt was made to separate surface effects from bulk effects in nanoparticles and to estimate the degree of inversion of the Zn_2SnO_4 nanophase.

The XPS method was applied to determine the macroscopic chemical composition of the outermost atom layers of the as-synthesized product. The results of XPS investigations excluded

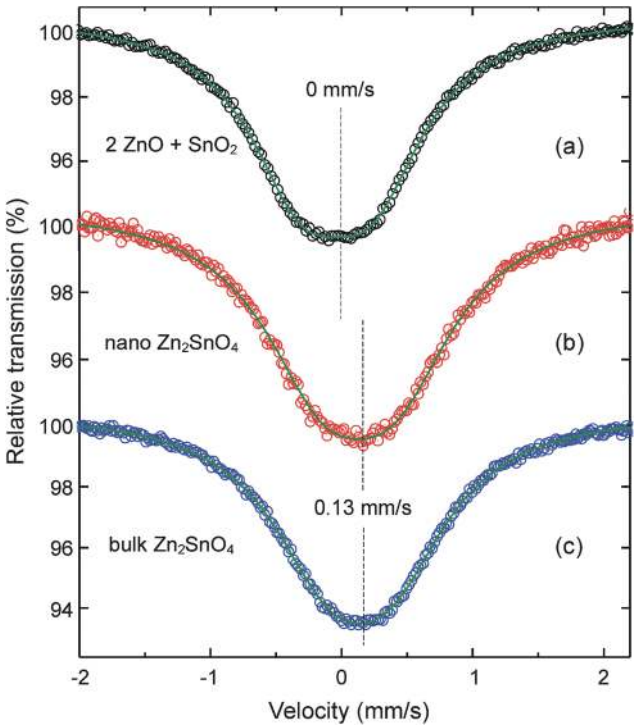

Fig. 8 ^{119}Sn Mössbauer spectra with the indicated central shifts for (a) the initial $2ZnO + SnO_2$ mixture, (b) mechanosynthesized Zn_2SnO_4, and (c) bulk Zn_2SnO_4. A Lorentzian line half-width of 0.55 mm s^{-1} resulting from the fit of the spectrum of bulk Zn_2SnO_4 was chosen for the fit of the spectrum of mechanosynthesized Zn_2SnO_4.

the presence of chemical elements originating from the abrasion of the milling tools (vial and balls made of WC) in the mechanosynthesized sample; Zn, Sn and O were the only elemental components detected. The quantitative analysis of the XPS data revealed that the mechanosynthesized nanostannate is chemically homogeneous with the Zn/Sn atomic ratio being 2. As clearly shown in Fig. 9, the mechanically induced formation reaction manifests itself by the shift of the Zn $2p_{3/2}$ signal in the XPS spectra: for the $2ZnO + SnO_2$ educt mixture, the Zn $2p_{3/2}$ signal is located at 1021.4 eV, whereas it is centred at 1021.9 eV for both mechanosynthesized and conventionally prepared Zn_2SnO_4.

In addition to XPS experiments, we carried out further EDX and the high-angle annular dark-field (HAADF) analyses of the mechanosynthesized product. The HAADF micrograph of the nanomaterial taken in the STEM mode (Fig. 10a) shows brightness variations just due to variations in specimen thickness, as do the elemental maps that monitor the local Kα X-ray emission from zinc and oxygen as well as the Lα X-ray emission from tin (Fig. 10b–d). The results of these semi-quantitative and microscopic measurements support the findings of XPS studies: the HAADF analysis hints to a homogeneous distribution of the constituent elements within agglomerated grains of the mechanosynthesized material. Similarly, as can be seen in the representative EDX spectrum (Fig. 10e), Zn, Sn and O were the only elemental components and no impurity was detected in the sample. Note that the spectral lines corresponding to Cu and C in the EDX spectrum originate from the copper-supported carbon grid.

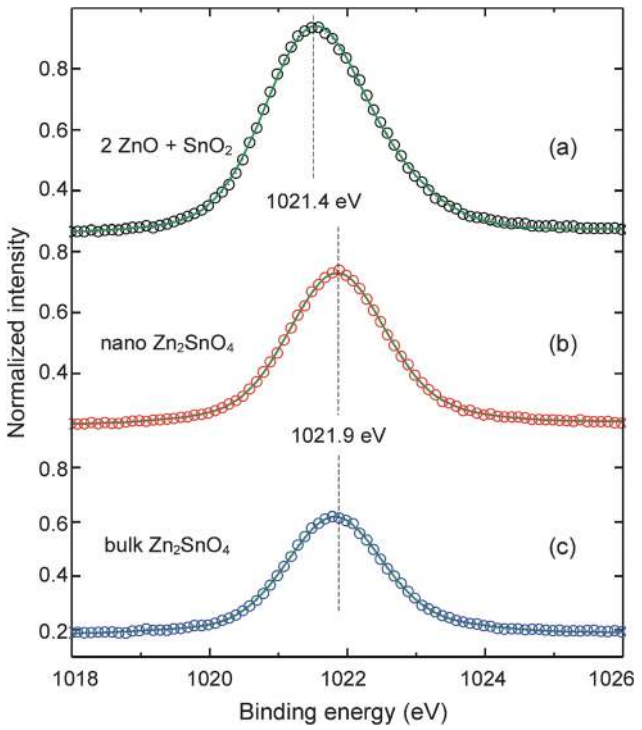

Fig. 9 The Zn $2p_{3/2}$ signal in the XPS spectra of (a) the initial $2ZnO + SnO_2$ mixture, (b) mechanosynthesized Zn_2SnO_4, and (c) bulk Zn_2SnO_4 prepared by the conventional thermal route. The positions of the XPS signals are indicated in the figure.

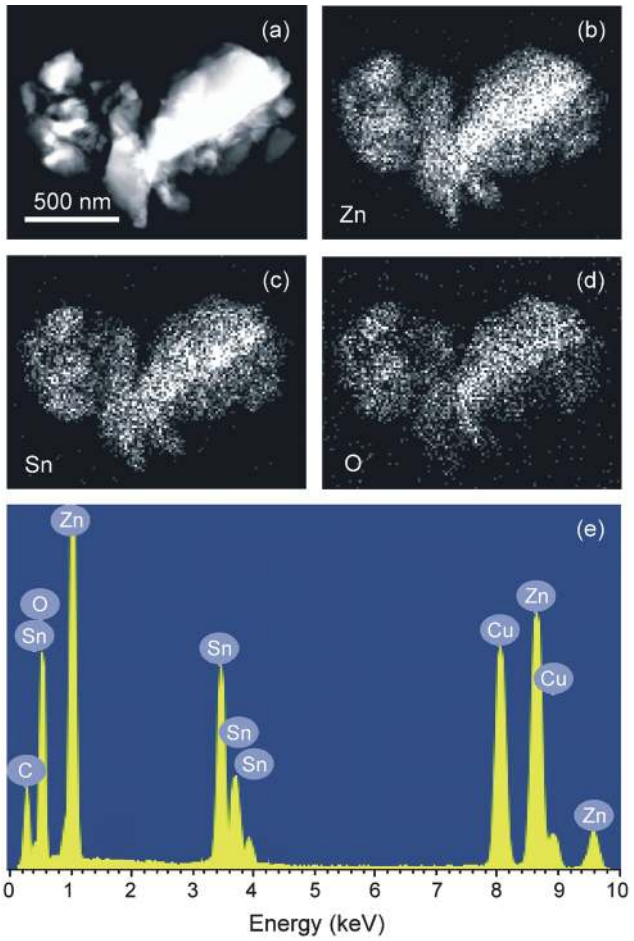

Fig. 10 (a) HAADF micrograph of mechanosynthesized Zn_2SnO_4 taken in the STEM mode. Micrographs showing distribution of the elements (b) zinc, (c) tin, and (d) oxygen within grains of the mechanosynthesized material. Bright contrasts represent high element concentrations. (e) EDX spectrum of nanocrystalline mechanosynthesized Zn_2SnO_4.

Conclusions

Zn_2SnO_4 spinel nanoparticles with an average size of about 26 nm have been prepared from binary oxide precursors by mechanosynthesis at ambient temperature. The mechanochemical route to the Zn_2SnO_4 nanospinel is completed after a relatively short time of 4 h. The present mechanochemical reaction, followed by XRD, ^{119}Sn MAS NMR, Raman spectroscopy, ^{119}Sn Mössbauer spectroscopy, and XPS, represents a one-step, high-yield, and low-temperature procedure for the synthesis of Zn_2SnO_4. On the basis of the results of high-resolution TEM investigations, it is concluded that the mechanosynthesized stannate nanoparticles possess a non-uniform configuration consisting of an ordered core surrounded by a disordered surface shell region. The comparative spectroscopic studies of bulk and nanocrystalline Zn_2SnO_4 enable us to separate surface effects from bulk effects in mechanosynthesized nanoparticles. The volume fraction of the structurally disordered surface shell regions in the nanostannate is estimated to be about 50%. The findings hint at the far-from-equilibrium structural state of the as-prepared nanooxide, characterized by the disorder of Sn and

Zn cations over the available spinel lattice sites as well as by the presence of deformed polyhedra in the near-surface layers of nanoparticles. Thus, the inner core of Zn_2SnO_4 nanoparticles possesses the fully inverse spinel structure, whereas the surface shell is disordered due to a nonequilibrium cation distribution and a broadly distorted local environment around the cations.

Acknowledgements

The present work was supported by the DFG in the framework of the Priority Program "*Crystalline Nonequilibrium Phases*" (SPP 1415). Partial support by the NSF and the VEGA (2/0174/11) is gratefully acknowledged. The authors also thank the BMBF and the DFG Center for Functional Nanostructures (CFN) at the Karlsruhe Institute of Technology for the support.

Notes and references

1 X.-Y. Liu, H.-W. Zheng, Z.-L. Zhang, X.-S. Liu, R.-Q. Wan and W.-F. Zhang, *J. Mater. Chem.*, 2011, **21**, 4108; C. Pang, B. Yan, L. Liao, B. Liu, Z. Zheng, T. Wu, H. Sun and T. Yu, *Nanotechnology*, 2010, **21**, 465706.
2 R. C. Singh, O. Singh, M. P. Singh, P. S. Chandi and R. Thangaraj, *Mater. Res. Bull.*, 2010, **45**, 1162; J. H. Yu and G. M. Choi, *J. Electroceram.*, 2002, **8**, 249.
3 A. Kurz, K. Brakecha, J. Puetz and M. A. Aegerter, *Thin Solid Films*, 2006, **502**, 212; Y. Sato, J. Kiyohara, A. Hasegawa, T. Hattori, M. Ishida, N. Hamada, N. Oka and Y. Shigesato, *Thin Solid Films*, 2009, **518**, 1304; M. Tsaroucha, Y. Aksu, E. Irran and M. Driess, *Chem. Mater.*, 2011, **23**, 2428.
4 T. Lana-Villarrea, G. Boschloo and A. Hagfeldt, *J. Phys. Chem. C*, 2007, **111**, 5549; B. Tan, E. Toman, Y. Li and Y. Wu, *J. Am. Chem. Soc.*, 2007, **129**, 4162.
5 S. M. Becker, M. Scheuermann, V. Šepelák, A. Eichhöfer, D. Chen, R. Mönig, A. S. Ulrich, H. Hahn and S. Indris, *Phys. Chem. Chem. Phys.*, 2011, **13**, 19624; J.-W. Lee and C.-H. Lee, *J. Supercrit. Fluids*, 2010, **55**, 252; X. J. Zhu, L. M. Geng, F. Q. Zhang, Y. X. Liu and L. B. Cheng, *J. Power Sources*, 2009, **189**, 828; A. Rong, X. P. Gao, G. R. Li, T. Y. Yan, H. Y. Zhu, J. Q. Qu and D. Y. Song, *J. Phys. Chem. B*, 2006, **110**, 14754.
6 E. L. Foletto, S. L. Jahn and R. F. P. M. Moreira, *J. Appl. Electrochem.*, 2010, **40**, 59; A. A. Firooz, A. R. Mahjoub, A. A. Khodadadi and M. Movahedi, *Chem. Eng. J.*, 2010, **165**, 735; Z. Ai, S. Lee, Y. Huang, W. Ho and L. Zhang, *J. Hazard. Mater.*, 2010, **179**, 141; X. Fu, X. Wang, J. Long, Z. Ding, T. Yan, G. Zhang, Z. Zhang, H. Lin and X. Fu, *J. Solid State Chem.*, 2009, **182**, 517; J. Zeng, M. Xin, K. Li, H. Wang, H. Yan and W. Zhang, *J. Phys. Chem. C*, 2008, **112**, 4159.
7 T. J. Coutts, D. L. Young, X. Li, W. P. Mulligan and X. Wu, *J. Vac. Sci. Technol., A*, 2000, **18**, 2646.
8 Joint Committee on Powder Diffraction, *Standards (JCPDS) Powder Diffraction File (PDF)*, International Centre for Diffraction Data, Newton Square, PA, 2004.
9 V. Šepelák, I. Bergmann, S. Indris, A. Feldhoff, H. Hahn, K. D. Becker, C. P. Grey and P. Heitjans, *J. Mater. Chem.*, 2011, **21**, 8332.
10 A. Navrotsky, *Physics and Chemistry of Earth Materials*, Cambridge University Press, Cambridge, 1994.
11 T. Hashemi, H. M. Al-Allak, J. Illingsworth, A. W. Brinkman and J. Woods, *J. Mater. Sci. Lett.*, 1990, **9**, 776; I. Stambolova, A. Toneva, V. Blaskov, D. Radev, Ya. Tsvetanova, S. Vassilev and P. Peshev, *J. Alloys Compd.*, 2005, **391**, L1; J.-W. Zhao, L.-R. Qin and L.-D. Zhang, *Solid State Commun.*, 2007, **141**, 663.
12 X. Hou, Q. Cheng, Y. Bai and W. F. Zhang, *Solid State Ionics*, 2010, **181**, 631.
13 E. Avvakumov, M. Senna and N. Kosova, *Soft Mechanochemical Synthesis: a Basis for New Chemical Technologies*, Kluwer Academic Publishers, Boston, 2001; V. V. Boldyrev, *Russ. Chem. Rev.*, 2006, **75**, 177; S. Kipp, V. Šepelák and K. D. Becker, *Chem. Unserer Zeit*, 2005, **39**, 384; B. Kubias, M. J. G. Fait and R. Schlögl, Mechanochemical Methods, in *Handbook of Heterogeneous Catalysis*, ed. G. Ertl, H. Knözinger, F. Schüth and J. Weitkamp, Wiley-VCH, Weinheim, 2008, vol. 1; F. Delogu and G. Mulas, *Experimental and Theoretical Studies in Modern Mechanochemistry*, Transworld Research Network, Kerala, 2010; S. L. James, C. J. Adams, C. Bolm, D. Braga, P. Collier, T. Friščić, F. Grepioni, K. D. M. Harris, G. Hyett, W. Jones, A. Krebs, J. Mack, L. Maini, A. G. Orpen, I. P. Parkin, W. C. Shearouse, J. W. Steed and D. C. Waddell, *Chem. Soc. Rev.*, 2012, **41**, 413.
14 V. Šepelák, K. D. Becker, I. Bergmann, S. Suzuki, S. Indris, A. Feldhoff, P. Heitjans and C. P. Grey, *Chem. Mater.*, 2009, **21**, 2518.
15 F. J. Berry, P. Wynn, J. Jiang and S. Mørup, *J. Mater. Sci.*, 2001, **36**, 3637.
16 N. Nikolić, T. Srećković and M. M. Ristić, *J. Eur. Ceram. Soc.*, 2001, **21**, 2071; N. Nikolić, Z. Marinković and T. Srećković, *J. Mater. Sci.*, 2004, **39**, 5239; T. Ivetić, Z. Vuković, M. V. Nikolić, V. B. Pavlović, J. R. Nikolić, D. Minić and M. M. Ristić, *Ceram. Int.*, 2008, **34**, 639.
17 V. Šepelák, A. Feldhoff, P. Heitjans, F. Krumeich, D. Menzel, F. J. Litterst, I. Bergmann and K. D. Becker, *Chem. Mater.*, 2006, **18**, 3057; V. Šepelák, I. Bergmann, A. Feldhoff, P. Heitjans, F. Krumeich, D. Menzel, F. J. Litterst, S. J. Campbell and K. D. Becker, *J. Phys. Chem. C*, 2007, **111**, 5026.
18 L. J. Berchmans, M. Myndyk, K. L. Da Silva, A. Feldhoff, J. Šubrt, P. Heitjans, K. D. Becker and V. Šepelák, *J. Alloys Compd.*, 2010, **500**, 68.
19 K. L. Da Silva, D. Menzel, A. Feldhoff, C. Kübel, M. Bruns, A. Paesano, Jr, A. Düvel, M. Wilkening, M. Ghafari, H. Hahn, F. J. Litterst, P. Heitjans, K. D. Becker and V. Šepelák, *J. Phys. Chem. C*, 2011, **115**, 7209.
20 A. Düvel, M. Wilkening, R. Uecker, S. Wegner, V. Šepelák and P. Heitjans, *Phys. Chem. Chem. Phys.*, 2010, **12**, 11251; M. J. N. Isfahani, M. Myndyk, V. Šepelák and J. Amighian, *J. Alloys Compd.*, 2009, **470**, 434; V. Šepelák, M. Menzel, I. Bergmann, M. Wiebcke, F. Krumeich and K. D. Becker, *J. Magn. Magn. Mater.*, 2004, **272–276**, 1616; V. Šepelák, S. Wissmann and K. D. Becker, *J. Magn. Magn. Mater.*, 1999, **203**, 135; P. Druska, U. Steinike and V. Šepelák, *J. Solid State Chem.*, 1999, **146**, 13; V. Šepelák, U. Steinike, D. C. Uecker, S. Wissmann and K. D. Becker, *J. Solid State Chem.*, 1998, **135**, 52.
21 S. Indris, M. Scheuermann, S. M. Becker, V. Šepelák, R. Kruk, J. Suffner, F. Gyger, C. Feldmann, A. S. Ulrich and H. Hahn, *J. Phys. Chem. C*, 2011, **115**, 6433; M. Achimovičová, K. L. Da Silva, N. Daneu, A. Rečnik, S. Indris, H. Hain, M. Scheuermann, H. Hahn and V. Šepelák, *J. Mater. Chem.*, 2011, **21**, 5873.
22 V. Šepelák, I. Bergmann, A. Feldhoff, F. J. Litterst, K. D. Becker, J. M. Cadogan, M. Hofmann, M. Hoelzel, J. L. Wang, M. Avdeev and S. J. Campbell, *Hyperfine Interact.*, 2010, **198**, 67; V. Šepelák, M. J. N. Isfahani, M. Myndyk, M. Ghafari, A. Feldhoff and K. D. Becker, *Hyperfine Interact.*, 2011, **202**, 39.
23 K. Brandenburg and H. Putz, *Diamond—Crystal and Molecular Structure Visualization Software, Version 3.0a*, Crystal Impact GbR, Bonn, Germany, 2004.
24 N. J. Clayden, C. M. Dobson and A. Fern, *J. Chem. Soc., Dalton Trans.*, 1989, 843.
25 K. Lagarec and D. G. Rancourt, *Recoil—Mössbauer Spectral Analysis Software for Windows, Version 1.02*, Department of Physics, University of Ottawa, Ottawa, ON, 1998.
26 K. L. Parry, A. G. Shard, R. D. Short, R. G. White, J. D. Whittle and A. Wright, *Surf. Interface Anal.*, 2006, **38**, 1497.
27 P. Heitjans, M. Masoud, A. Feldhoff and M. Wilkening, *Faraday Discuss.*, 2007, **134**, 67; P. Heitjans and M. Wilkening, *MRS Bull.*, 2009, **34**, 915.
28 P. Heitjans and S. Indris, *J. Phys.: Condens. Matter*, 2003, **15**, R1257; P. Heitjans and S. Indris, *J. Mater. Sci.*, 2004, **39**, 5091; A. Kuhn, E. Tobschall and P. Heitjans, *Z. Phys. Chem.*, 2009, **223**, 1359.
29 M. Muroi, R. Street, P. G. McCormick and J. Amighian, *Phys. Rev. B: Condens. Matter*, 2001, **63**, 184414; Y. D. Zhang, S. H. Ge, H. Zhang, S. Hui, J. I. Budnick, W. A. Hines, M. J. Yacaman and M. Miki, *J. Appl. Phys.*, 2004, **95**, 7130.
30 C. P. Grey, C. M. Dobson, A. K. Cheetham and R. J. B. Jakeman, *J. Am. Chem. Soc.*, 1989, **111**, 505; *Multinuclear Solid-State NMR of Inorganic Materials*, ed. K. J. D. MacKenzie, Pergamon Materials Series, Amsterdam, 2002, vol. 6; A. W. MacGregor, L. A. O'Dell

and R. W. Schurko, *J. Magn. Reson.*, 2011, **208**, 103; V. I. Bakhmutov, *Chem. Rev.*, 2011, **111**, 530.
31 C. Cossement, J. Darville, J.-M. Gilles, J. B. Nagy, C. Fernandez and J.-P. Amoureux, *Magn. Reson. Chem.*, 1992, **30**, 263.
32 D. L. Young, D. L. Williamson and T. J. Coutts, *J. Appl. Phys.*, 2002, **91**, 1464; D. L. Young, H. Moutinho, Y. Yan and T. J. Coutts, *J. Appl. Phys.*, 2002, **92**, 310.
33 V. Šepelák, S. Indris, I. Bergmann, A. Feldhoff, K. D. Becker and P. Heitjans, *Solid State Ionics*, 2006, **177**, 2487; V. Šepelák, S. Indris, P. Heitjans and K. D. Becker, *J. Alloys Compd.*, 2007, **434–435**, 776.
34 V. Šepelák, I. Bergmann, A. Diekmann, P. Heitjans and K. D. Becker, *Rev. Adv. Mater. Sci.*, 2008, **18**, 349.
35 N. V. Porotnikov, V. G. Savenko and O. V. Sidorova, *Russ. J. Inorg. Chem.*, 1983, **28**, 983.
36 M. V. Nikolić, T. Ivetić, D. L. Young, K. M. Paraskevopoulos, T. T. Zorba, V. Blagojević, P. M. Nikolić, D. Vasiljević-Radović and M. M. Ristić, *Mater. Sci. Eng., B*, 2007, **138**, 7.
37 M. Lazzeri and P. Thibaudeau, *Phys. Rev. B: Condens. Matter Mater. Phys.*, 2006, **74**, 140301(R).
38 Z. Wang, P. Lazor, S. K. Saxena and H. S. C. O'Neill, *Mater. Res. Bull.*, 2002, **37**, 1589.
39 X. Shen, J. Shen, S. J. You, L. X. Yang, L. Y. Tang, Y. C. Li, J. Liu, H. Yang, K. Zhu, Y. L. Liu, W. Y. Zhou, C. Q. Jin, R. C. Yu and S. S. Xie, *J. Appl. Phys.*, 2009, **106**, 113523.
40 P. Chandramohan, M. P. Srinivasan, S. Velmurugan and S. V. Narasimhan, *J. Solid State Chem.*, 2011, **184**, 89.
41 S. A. T. Redfern, R. J. Harrison, H. S. C. O'Neill and D. R. R. Wood, *Am. Mineral.*, 1999, **84**, 299.
42 Z. Wang, P. Lazor, S. K. Saxena and G. Artioli, *J. Solid State Chem.*, 2002, **165**, 165.
43 K. E. Sickafus, A. C. Larson, N. Y. M. Nastasi, G. W. Hollenberg, F. A. Garner and R. C. Bradt, *J. Nucl. Mater.*, 1995, **219**, 128; T. Soeda, S. Matsumura, C. Kinoshita and N. J. Zaluzec, *J. Nucl. Mater.*, 2000, **283–287**, 952.
44 V. Šepelák, K. Tkáčová and A. I. Rykov, *Cryst. Res. Technol.*, 1993, **28**, 53; V. Šepelák, D. Baabe, F. J. Litterst and K. D. Becker, *J. Appl.Phys.*, 2000, **88**, 5884; V. Šepelák, D. Baabe and K. D. Becker, *J. Mater. Synth. Process.*, 2000, **8**, 333; V. Šepelák, D. Schultze, F. Krumeich, U. Steinike and K. D. Becker, *Solid State Ionics*, 2001, **141–142**, 677; V. Šepelák, D. Baabe, D. Mienert, D. Schultze, F. Krumeich, F. J. Litterst and K. D. Becker, *J. Magn. Magn. Mater.*, 2003, **257**, 377; V. Šepelák and K. D. Becker, *Mater. Sci. Eng., A*, 2004, **375–377**, 861; V. Sreeja, T. S. Smitha, D. Nand, T. G. Ajithkumar and P. A. Joy, *J. Phys. Chem. C*, 2008, **112**, 14737.
45 H. Cynn, S. K. Sharma, T. F. Conney and M. Nicol, *Phys. Rev. B: Condens. Matter*, 1992, **45**, 500.
46 A. Weibel, R. Bouchet, S. L. P. Savin, A. V. Chadwick, P. E. Lippens, M. Womes and P. Knauth, *Phys. Chem. Chem. Phys.*, 2006, **7**, 2377.

